Diffractive slit patterns for focusing surface plasmon polaritons

Hwi Kim and Byoungho Lee*

National Creative Research Center for Active Plasmonics Application Systems,
Inter-University Semiconductor Research Center and School of Electrical Engineering,
Seoul National University, Seoul 151-744, Korea
**Corresponding author: byoungho@snu.ac.kr;http://oeqelab.snu.ac.kr*

Abstract: We propose a design method of diffractive slit patterns for focusing surface plasmon polaritons. A scalar model of surface plasmon polariton excitation and interference is adopted, based on which the design method of diffractive slit patterns is built up. The validity of the proposed scalar model-based design is discussed through the comparison of the simulation results of the scalar model and the rigorous three-dimensional vectorial electromagnetic model using the rigorous coupled wave analysis.

OCIS codes: (240.6680) Surface plasmons; (250.5300) Photonic integrated circuits.

References and links

1. W. L. Barnes, A. Dereux, and T. W. Ebbesen, "Surface plasmon subwavelength optics," Nature **424**, 824-830 (2003).
2. E. Ozbay, "Plasmonics: Merging photonics and electronics at nanoscale dimensions," Science **311**, 189-193 (2006).
3. P. Berini, R. Charbonneau, and N. Lahoud, "Long-range surface plasmons on ultrathin membranes," Nano Lett. **7**, 1376-1380 (2007).
4. L. Yin, V. K. Vlasko-Vlasov, J. Pearson, J. M. Miller, J. Hua, U. Welp, D. E. Brown, and C. W. Kimball, "Subwavelength focusing and guiding of surface plasmons," Nano Lett. **5**, 1399-1402 (2005).
5. I. P. Radko, S. I. Bozhevolnyi, A. B. Evlyukhin, and A. Boltasseva, "Surface plasmon polariton beam focusing with parabolic nanoparticle chains," Opt. Express **15**, 6576-6582 (2007).
6. H. L. Offerhaus, B. van den Bergen, M. Escalante, F. B. Segerink, J. P. Korterik, and N. F. van Hulst, "Creating focused plasmons by noncollinear phasematching on functional gratings," Nano Lett. **5**, 2144-2148 (2005).
7. Z. Liu, J. M. Steele, W. Srituravanich, Y. Pikus, C. Sun, and X. Zhang, "Focusing surface plasmons with plasmonic lens," Nano Lett. **5**, 1726-1729 (2005).
8. Z. Liu, J. M. Steele, H. Lee, and X. Zhang, "Tuning the focus of a plasmonic lens by the incident angle," Appl. Phys. Lett. **88**, 121108 (2006).
9. H. Kim, J. Hahn, and B. Lee,"Focusing properties of surface plasmon polariton floatig dielectric lenses," Opt. Express 16, 3049-3057 (2008).
10. L. Feng, K. A. Tetz, B. Slutsky, V. Lomakin, and Y. Fainman, "Fourier plasmonics: Diffractive focusing of in-plane surface plasmon polariton waves," Appl. Phys. Lett. **91**, 081101 (2007).
11. H. Kim, J. Hahn, and B. Lee, "Mathematical modeling of triangle-mesh-modeled three-dimensional surface objects for digital holography," Appl. Opt. **47**, D117-D127 (2008).
12. R. Zia and M. L. Brongersma, "Surface plasmon polariton analogue to Young's double-slit experiment," Nat. Nanotechnol. **2**, 426-429 (2007).
13. H. Kim, I.-M. Lee, and B. Lee, "Extended scattering-matrix method for efficient full parallel implementation of rigorous coupled-wave analysis," J. Opt. Soc. Am. A **24**, 2313-2327 (2007).
14. H. Kim and B. Lee, "Mathematical modeling of crossed nanophotonic structures with generalized scattering-matrix method and local Fourier modal analysis," J. Opt. Soc. Am. B **25**, 518-544 (2008).

1. Introduction

Surface plasmon polariton (SPP) is an electromagnetic surface mode coupled with surface conduction electrons at metal dielectric interfaces. SPP is considered to provide a unique way with which photonic systems can be integrated on nano scale chips in fusion with nanoelectronics [1-3]. Basic and advanced engineering functions as well as fundamental features of SPPs have been intensively researched. However there are still many challengeable problems in establishing basic functions for managing and controlling SPPs at the nano dimensions.

An important basic function is focusing SPPs. Since SPP is a surface bound mode, various surface nanostructures for focusing SPPs have been researched in many previous works [4-10]. Point-wise SPP generators such as subwavelength holes and dots are arrayed by the form of lens structures [4-6] to generate focused SPP patterns. Several surface dielectric structures can be used for focusing SPPs [9, 10]. The degrees of freedom for dynamic SPP focusing are also an important point in recent researches on SPP focusing [8, 9].

In this paper, we propose a design method of diffractive slit patterns for focusing SPPs based on diffractive optics concept [11]. A two-dimensional (2-D) scalar optics model of SPP excitation and interference [12] is adopted, based on which the design method of diffractive slit patterns is built up. The feasibility of multiple SPP focusing as well as single SPP focusing with the proposed method is examined.

The validity of the proposed scalar model-based design is discussed through the comparison of the simulation results of the scalar model and the rigorous three-dimensional vectorial electromagnetic model using the rigorous coupled wave analysis (RCWA) [13, 14].

In Section 2, design method of diffractive slit patterns and scalar model of surface plasmon polariton interference are described. In Section 3, numerical results of the RCWA are presented and discussed. In Section 4, concluding remarks are given.

2. Diffractive slit patterns and scalar model of surface plasmon polariton interference

In this section, the design method of diffractive slit patterns for focusing SPPs is described and practical design examples are presented. The design is based on the simple scalar model of SPP interference, of which validity will be discussed with the comparison with the numerical results of vectorial electromagnetic simulation using the RCWA in Section 3.

Let us consider the wave front of superposition field of multiple 2-D SPP point sources give by

$$\begin{aligned} F(x,y) &= \sum_m \exp\left(jk_{SPP}\sqrt{(x-x_m)^2+(y-y_m)^2} \right) \\ &= \sum_m \exp\left(\left(jk_{SPP}^r - k_{SPP}^i \right)\sqrt{(x-x_m)^2+(y-y_m)^2} \right), \end{aligned} \tag{1a}$$

where (x_m, y_m) is the spot center of a point sources. k_{SPP} is the wavenumber of SPP given by

$$k_{SPP} = \frac{2\pi}{\lambda}\sqrt{\frac{\varepsilon_a\varepsilon_m}{\varepsilon_a+\varepsilon_m}} = \frac{2\pi}{\lambda_{SPP}}, \tag{1b}$$

where λ is free space wavelength, ε_a is the permittivity of air, ε_m is the permittivity of metal (Au) substrate, and λ_{SPP} is the SPP wavelength on air/metal interface. k_{SPP}^r and k_{SPP}^i are the real and imaginary parts of k_{SPP}. In general, SPP propagates with inherent damping due to the ohmic loss of metallic media, which is indicated by the term, k_{SPP}^i in Eq. (1a). In this paper, we assume that λ, ε_a, and ε_m are 650nm, 1, and $-9.8492 + j1.0572$, respectively. Then the SPP wavelength, λ_{SPP}, is given by $616.5\text{nm-j}3.7\text{nm}$. Let us define the complementary field $G(x,y)$ of $F(x,y)$ as

$$\begin{aligned} G(x,y) &= \sum_m \exp\left(\left(-jk_{SPP}^r + k_{SPP}^i \right)\sqrt{(x-x_m)^2+(y-y_m)^2} \right) \\ &= a(x,y)\exp\left(j\phi(x,y) \right), \end{aligned} \tag{2}$$

#94111 - $15.00 USD Received 20 Mar 2008; revised 17 May 2008; accepted 30 May 2008; published 3 Jun 2008

where $a(x,y)$ and $\phi(x,y)$ are the amplitude and phase functions of the composite optical field $G(x,y)$. $G(x,y)$ is composed of the circular wave components with the counterdirectional wavenumber, $-k_{SPP}$, that are exponentially increasing from the spot centers (x_m, y_m).

Let us define a concentric band (on the metal surface) with the outer and inner radii of R_1 and R_2. Then let the intersections of the constant phase contours of the phase function, $\phi(x,y)$ (for phase values of 0 and $-\pi$) and the concentric band be denoted by Ω^+ and Ω^-, respectively. Ω^+ and Ω^- are mathematically expressed by the set forms given, respectively, by

$$\Omega^+ = \left\{(x,y) \mid \phi(x,y) = 0 \text{ and } R_2 \le \sqrt{x^2+y^2} \le R_1\right\}, \tag{3a}$$

$$\Omega^- = \left\{(x,y) \mid \phi(x,y) = -\pi \text{ and } R_2 \le \sqrt{x^2+y^2} \le R_1\right\}. \tag{3b}$$

The diffractive slit patterns will be extracted from Ω^+ and Ω^-, of which subsets become a part of diffractive slit patterns for multiple SPP focal spots. In addition, let the amplitude profiles of Ω^+ and Ω^- be defined by A^+ and A^- as

$$\mathrm{A}^+ = \left\{a(x,y) \mid (x,y) \in \Omega^+\right\}, \tag{3c}$$

$$\mathrm{A}^- = \left\{a(x,y) \mid (x,y) \in \Omega^-\right\}, \tag{3d}$$

which will be used in the discussion on the amplitude damping of SPP fields in the latter part of this paper.

To understand the proposed design method, let us first consider the complementary field of a single SPP point source which is the simplest case of Eq. (2) given by

$$G(x,y) = \exp\left(-jk_{SPP}\sqrt{(x-x_c)^2+(y-y_c)^2}\right). \tag{4}$$

The phase distributions of two point sources with different origins, (x_c, y_c), at $(0,0)$ and $(1.5\mu\text{m}, 1.5\mu\text{m})$, are presented in Fig. 1(a) and 1(b), respectively. In this paper, R_1 and R_2 of the concentric band are chosen as $3.89\mu\text{m}$ and $R_1 - \lambda_{SPP}^r$, respectively, λ_{SPP}^r is the real part of λ_{SPP}. The rectangle region of $9\mu\text{m}\times 9\mu\text{m}$ size is concerned. In Fig. 1(c), the phase distribution of a composite field of two point sources with the centers at $(1.5\mu\text{m}, 1.5\mu\text{m})$ and $(-1.5\mu\text{m}, -1.5\mu\text{m})$ is shown. The amplitude profiles of Figs. 1(a), 1(b), and 1(c) are shown in Figs. 1(d), 1(e), and 1(f), respectively. The concentric band is indicated by white dashed lines in Figs. 1(a), 1(b) and 1(c) and by black dashed lines in Figs. 1(d), 1(e), and 1(f).

#94111 - \$15.00 USD Received 20 Mar 2008; revised 17 May 2008; accepted 30 May 2008; published 3 Jun 2008

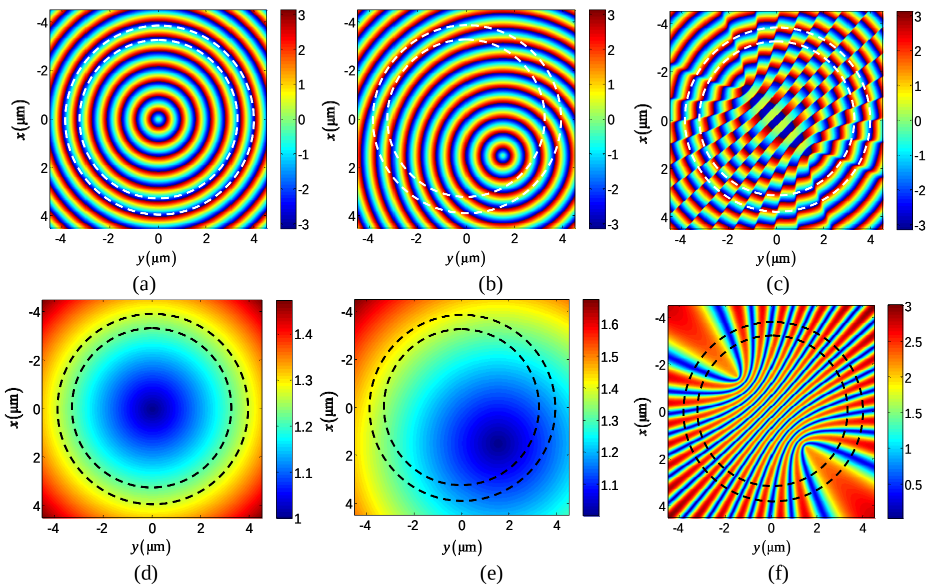

Fig. 1. Phase distributions of complementary single point sources with the centers (a) at $(x_c, y_c) = (0,0)$ and (b) at $(x_c, y_c) = (1.5\mu\text{m}, 1.5\mu\text{m})$. (c) Phase distribution of a composite field of two point sources with the centers at $(1.5\mu\text{m}, 1.5\mu\text{m})$ and $(-1.5\mu\text{m}, -1.5\mu\text{m})$. Amplitude distributions of complementary single point sources with the centers (d) at $(x_c, y_c) = (0,0)$ and (e) at $(x_c, y_c) = (1.5\mu\text{m}, 1.5\mu\text{m})$. (f) Amplitude distribution of a composite field of two point sources with the centers at $(1.5\mu\text{m}, 1.5\mu\text{m})$ and $(-1.5\mu\text{m}, -1.5\mu\text{m})$.

To figure out the meanings of Ω^+ and Ω^-, Ω^+ and Ω^- of a single 2-D point source with its center at $(0,0)$ are represented by the red circles in Figs. 2(a) and 2(c), respectively. In both figures, the concentric band is indicated by white dashed lines. If a subwavelength curved slit pattern is formed following the path of Ω^+ or Ω^- in a thin metal film placed on the *x*-*y* plane (*z*=0) and an *x*-directional polarization plane wave is normally incident on the backside of the metal film, SPPs excited on the front surface of the metal film by the curved slit propagate and produce complex interference patterns on the metal surface. In the cases shown in Fig. 2, it is expected for SPP to form a focused spot on the origin, $(0,0)$ because of the circular symmetry of the circular slit pattern. However, in understanding the SPP focusing, we should necessarily consider the polarity of SPP excitation. Because the incident optical field is *x*-directional linear polarized, the SPP excited on the slit in the region of $x \le 0$ and that in the region of $x > 0$ have different polarity, that is, π-phase difference. In Figs. 2(b) and 2(d), the plus and minus signs are used to visually indicate the polarity of SPP in the inner region in $x \le 0$ and in the inner region in $x > 0$, respectively. In the case of Ω^+, the plus-signed half circle and minus-signed half circle are denoted by a black and white half circles, respectively in Fig. 2(b), while in the case of Ω^- the plus signed half circle and minus-signed half circle are denoted by a white and black half circle, respectively, in Fig. 2(d).

#94111 - $15.00 USD Received 20 Mar 2008; revised 17 May 2008; accepted 30 May 2008; published 3 Jun 2008

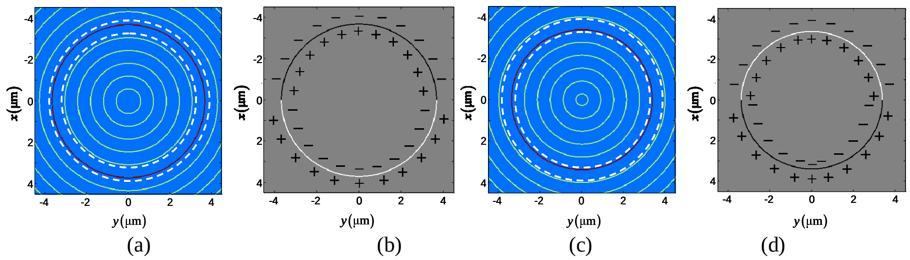

Fig. 2. (a). Ω^{+} of a point source with the center at the origin, (b) slit pattern extracted from Ω^{+} and SPP polarity, (c) Ω^{-} of the point source with the center at the origin, (d) slit pattern extracted from Ω^{-} and SPP polarity.

Before going further, let us adopt a simple scalar SPP excitation and propagation model [12] to simulate the interference effect of the slit patterns. Basically we assume that the slit curve is filled with continuous 2-D SPP point sources, of which the center is distributed on the slit. From simple physical intuition, we assume that the SPP excitation strength and the polarity are determined by the magnitude and the sign of the inner product of the outward normal vector of the slit curve and the polarization vector, which is the *x*-directional unit vector in this case. Then the SPP interference pattern, $U(x, y)$, is represented by

$$U(x,y)=\int_{C}\exp\left(jk_{SPP}\sqrt{(x-x')^{2}+(y-y')^{2}}\right)\mathbf{p}\cdot\mathbf{n}ds\,, \tag{5}$$

where the slit curve is denoted by C, $\mathbf{p}$ and $\mathbf{n}$ are the polarization vector of the illuminating plane wave and the outer normal vector of the slit curve C, and ds is the differential length along the slit curve C.

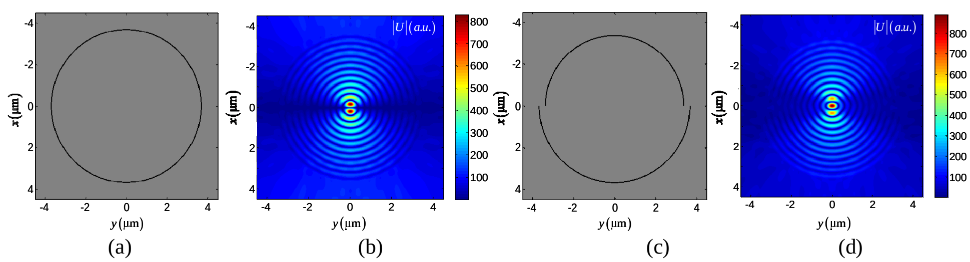

Fig. 3. Single SPP spot generation: (a) slit pattern without the compensation of the π-phase difference, (b) SPP interference pattern, (c) slit pattern with the compensation of the π-phase difference, (d) SPP interference pattern

In the case of the circle slit shown in Fig. 3(a), the SPP interference pattern is dual point SPP focus pattern as seen in Fig. 3(b). On the circle slit, because of the π-phase difference in SPPs excited on the upper part and lower part of the circle slit, the destructive interference occurs at the origin. Thus, we can see the dual point SPP focus pattern. However, if we make a slit by combining two half circles with different polarities, for example, the white half circle of Ω^{+} circle and the black half circle of Ω^{-}, we can make a slit pattern with the π-phase difference compensated. The resulting slit pattern and its SPP interference pattern are shown in Fig. 3(c) and 3(d), respectively. As shown in Fig. 3(d), at the origin, the constructive interference occurs. The maximum SPP field intensity around the focal point of the phase compensated slit is about 1.5 times higher than that of the circle slit without the compensation of the π-phase difference.

#94111 - $15.00 USD Received 20 Mar 2008; revised 17 May 2008; accepted 30 May 2008; published 3 Jun 2008

The slit pattern design concept described above can be extended to more general design procedure of diffractive slit patterns generating multiple SPP focal spots. From the general superposed field of Eq. (2), we can extract diffractive slit patterns to form multiple SPP focal spots at specific positions, (x_m, y_m). First, the intersection sets of the constant phase contours and the concentric band, Ω^+ and Ω^-, should be extracted, for which numerical calculations are necessary. This is the phase contour extraction stage. Second, the parity of SPP excitation is analyzed with the inspection of the sign of the inner product of the outward normal vector of the slit curve, $\mathbf{n}$, and the polarization vector, $\mathbf{p}$. The outward normal vector of the slit curve, $\mathbf{n}$, is obtained by the gradient vector of the phase function $\phi(x, y)$

$$\nabla\Omega^{\pm} = \left(\partial\phi(x,y)/\partial x, \partial\phi(x,y)/\partial y\right)_{(x,y)\in\Omega^{\pm}}, \tag{6a}$$

where $\phi(x, y)$ is given by

$$\phi(x,y) = -\tan^{-1}\left[\frac{\sum_m e^{k_{SPP}^i\sqrt{(x-x_m)^2+(y-y_m)^2}}\sin\left(k_{SPP}^r\sqrt{(x-x_m)^2+(y-y_m)^2}\right)}{\sum_m e^{k_{SPP}^i\sqrt{(x-x_m)^2+(y-y_m)^2}}\cos\left(k_{SPP}^r\sqrt{(x-x_m)^2+(y-y_m)^2}\right)}\right], \tag{6b}$$

and then $\partial\phi(x,y)/\partial x$ and $\partial\phi(x,y)/\partial y$ are obtained, respectively, as

$$\frac{\partial\phi(x,y)}{\partial x} = -\left(\cos\phi(x,y)\right)^2\frac{\partial}{\partial x}\left[\frac{\sum_m e^{k_{SPP}^i\sqrt{(x-x_m)^2+(y-y_m)^2}}\sin\left(k_{SPP}^r\sqrt{(x-x_m)^2+(y-y_m)^2}\right)}{\sum_m e^{k_{SPP}^i\sqrt{(x-x_m)^2+(y-y_m)^2}}\cos\left(k_{SPP}^r\sqrt{(x-x_m)^2+(y-y_m)^2}\right)}\right], \tag{6c}$$

$$\frac{\partial\phi(x,y)}{\partial y} = -\left(\cos\phi(x,y)\right)^2\frac{\partial}{\partial y}\left[\frac{\sum_m e^{k_{SPP}^i\sqrt{(x-x_m)^2+(y-y_m)^2}}\sin\left(k_{SPP}^r\sqrt{(x-x_m)^2+(y-y_m)^2}\right)}{\sum_m e^{k_{SPP}^i\sqrt{(x-x_m)^2+(y-y_m)^2}}\cos\left(k_{SPP}^r\sqrt{(x-x_m)^2+(y-y_m)^2}\right)}\right]. \tag{6d}$$

Then, the outward normal vector $\mathbf{n}$ is given by the normalized gradient vector $\mathbf{n} = \nabla\Omega^{\pm}/\left|\nabla\Omega^{\pm}\right|$. Let the x-directional linear polarization vector of the incident optical field be denoted by $\mathbf{p} = (1, 0)$. The sign of the inner product of $\mathbf{p}$ and the gradient vector $\nabla\Omega^{\pm}$ may be plus or minus. According to the sign of this inner product, the Ω^+ is divided into Ω_p^+ and Ω_n^+ and Ω^- is divided into Ω_p^- and Ω_n^-. The subsets, Ω_p^+, Ω_n^+, Ω_p^-, and Ω_n^-, are defined, respectively, as

$$\Omega_p^+ = \left\{(x,y) \mid \phi(x,y) = 0 \text{ and } \nabla\Omega^+\cdot\mathbf{p} \geq 0\right\}, \tag{7a}$$

$$\Omega_n^+ = \left\{(x,y) \mid \phi(x,y) = 0 \text{ and } \nabla\Omega^+\cdot\mathbf{p} < 0\right\}, \tag{7b}$$

$$\Omega_p^- = \left\{(x,y) \mid \phi(x,y) = -\pi \text{ and } \nabla\Omega^-\cdot\mathbf{p} \geq 0\right\}, \tag{7c}$$

$$\Omega_n^- = \left\{(x,y) \mid \phi(x,y) = -\pi \text{ and } \nabla\Omega^-\cdot\mathbf{p} < 0\right\}. \tag{7d}$$

The slit pattern with the π-phase difference compensated is obtained as the unions of the subsets, $\Omega_p^+ \cup \Omega_n^-$ or $\Omega_p^- \cup \Omega_n^+$. The slit pattern shown in Fig. 3(c) is $\Omega_p^+ \cup \Omega_n^-$. We can also

#94111 - $15.00 USD Received 20 Mar 2008; revised 17 May 2008; accepted 30 May 2008; published 3 Jun 2008

define the amplitude profiles of Ω_p^+, Ω_n^+, Ω_p^-, and Ω_n^- by A_p^+, A_n^+, A_p^-, and A_n^-, respectively, by the same manner of the definition of Eqs. (3c) and (3d).

Let us design a slit pattern to generate a SPP focal spot at an off-origin point, $(1.5\mu m, 1.5\mu m)$, of which phase distribution is shown in Fig. 1(b). The sets, Ω^+ and Ω^-, of this case are presented by the red lines in Figs. 4(a) and 4(d), respectively. The polarities of the SPP excitation are distinguished by white and black curves in Figs. 4(b) and 4(e) according to the above stated method. In Fig. 4(c) and 4(d), the amplitude profiles of Ω^+ and Ω^- defined in Eqs. (3c) and (3d) are shown, respectively.

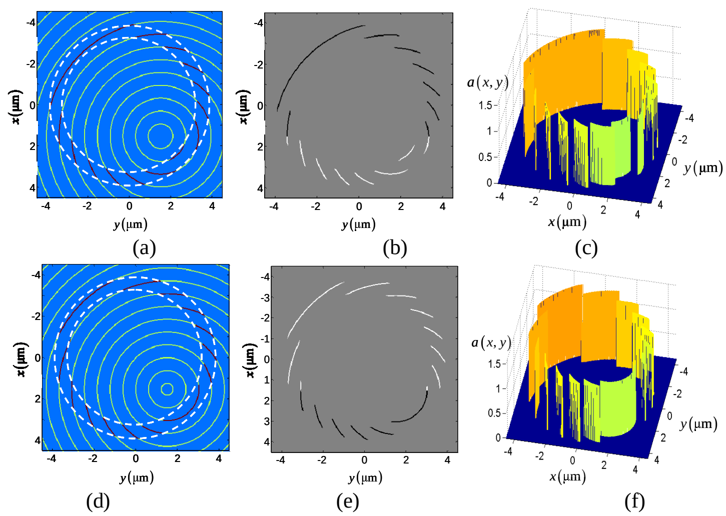

Fig. 4. (a). Ω^+ of a point source with the center at the off-origin $(1.5\mu m, 1.5\mu m)$ (indicated by red lines), (b) slit pattern extracted from Ω^+ and SPP polarity (Ω_p^+ is while and Ω_n^+ is black), (c) A^+; amplitude profile of Ω^+, (d) Ω^- of the point source with the center at the off-origin (indicated by red lines), (e) slit pattern extracted from Ω^- and SPP polarity (Ω_p^- is black and Ω_n^- is white), (f) A^-; amplitude profile of Ω^-.

Here, we give a discussion on the damping effect of SPP ($k_{SPP}^i \neq 0$) and its consideration in the proposed slit design method. In the framework addressed above, the complementary field $G(x, y)$ with both counterdirectional wavenumber and exponential amplification property is used to extract the diffractive slit pattern. If SPP is excited on the extracted slit C with the definite amplitude profile proportional to the amplified amplitude profile $a(x, y)$, the amplitude profile $a(x, y)$ would effectively compensate the damping loss of SPP propagating along the metal/dielectric interface and as a result, we may obtain desired SPP focusing profiles. In this case, the SPP interference pattern, $U(x, y)$, is represented by

$$U(x, y) = \int_C a(x, y) \exp\left(jk_{SPP} \sqrt{(x - x')^2 + (y - y')^2} \right) ds . \tag{8a}$$

However, under the assumption of the linear polarization excitation, the polarization effect on the SPP excitation strength and polarity should be taken into account. Thus, under the intuition that the SPP excitation strength is proportional to the inner product, $\mathbf{p} \cdot \mathbf{n}$, of the polarization, $\mathbf{p}$, and the outer normal vector, $\mathbf{n}$, at a local point on the slit as shown in Eq. (5), the SPP interference pattern should take the form

#94111 - \$15.00 USD Received 20 Mar 2008; revised 17 May 2008; accepted 30 May 2008; published 3 Jun 2008

$$U(x,y)=\int_C a(x,y)\exp\left(jk_{SPP}\sqrt{(x-x')^2+(y-y')^2}\right)\mathbf{p}\cdot\mathbf{n}ds\ . \tag{8b}$$

This notion can be extended to the cases of other excitation conditions such as elliptical polarization excitation. In this case, the polarization vector $\mathbf{p}$ is not a constant vector but a spatial vector function. Since the proposed slit pattern design method is based on the simple scalar model, the polarization of the incident beam is not taken into account in the design stage. In the analysis of the constructed SPP field distribution, the polarization effect is considered as shown in Eq. (8b), where the polarization vector $\mathbf{p}$ is a general spatial polarization vector function.

In Eq. (8b), the SPP excitation strength is assumed to be modulated by the amplitude function $a(x,y)$. However, in practice, it would be very difficult to realize the SPP amplitude modulation profiled by $a(x,y)$. This problem requires further research. In diffractive optics, it is well known that the diffractive or interferometric optical field synthesis is more strongly influenced by phase distribution than by amplitude distribution. In diffractive field synthesis problems [11], the amplitude profile is usually set to a constant due to practical reasons (see Sec. 4 in ref. [11]). Although the amplitude profile is less effective on the field synthesis profile than the phase profile, this constant amplitude clipping induces some background noise and slight signal degradation.

In the SPP focal spot synthesis using the diffractive slit patterns, the same concept is applicable. In the simulations of this paper, the relative amplitude profile variation is ranged from 1 to 1.5. In this case, the effect of the constant amplitude clipping is acceptable. Thus, the SPP interference pattern is represented by Eq. (5).

As the radii, R_1 and R_2, of a concentric band (on the metal surface) increase and the focal spot pattern becomes complex, the amount of unevenness of the amplitude profile $a(x,y)$ becomes larger and, as a result, the influence of the amplitude profile will be significant. The phase only optical slit pattern design with the constant amplitude profile requires specifically devised nonlinear optimization algorithm, which is an advanced problem that is posed from this paper. The simple and efficient scalar model such as Eq. (5) is inevitable for building up the optimal design method of phase only diffractive slit pattern.

In Figs. 5(a) and 5(c), the slit patterns without and with the π-phase difference compensation are shown, respectively. The resulting SPP interference patterns from respective slit patterns with the uniform SPP excitation on the slit curve are presented in Figs. 5(b) and 5(d), respectively. In the case of the circle slit shown in Fig. 5(a), the resulting SPP interference pattern is dual point SPP focus pattern as seen in Fig. 5(b). Because of the π-phase difference between SPPs excited on the Ω_p^+ and Ω_n^+ parts of the slit, the destructive interference occurs at the focal point. However, if we make a slit by combining the half circles with different polarities, for example, the white lined part of Ω^+ and the white lined part of Ω^-, that is, using $\Omega_p^+\cup\Omega_n^-$, we can make the slit pattern with the π-phase difference compensated. The resulting slit pattern and its resulting SPP interference pattern are shown in Figs. 5(c) and 5(d), respectively. As shown in Fig. 5(d), at the focal point, the constructive interference occurs.

#94111 - $15.00 USD Received 20 Mar 2008; revised 17 May 2008; accepted 30 May 2008; published 3 Jun 2008

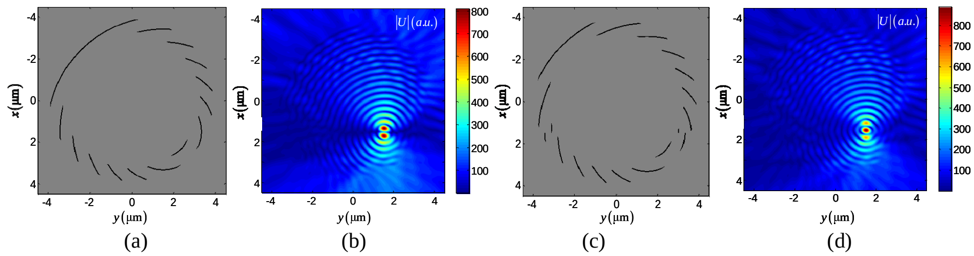

Fig. 5. Single SPP spot generation: (a) slit pattern without the compensation of the π -phase difference, (b) SPP interference pattern, (c) slit pattern with the compensation of the π -phase difference, (d) SPP interference pattern.

Let us consider a slightly complex slit pattern to generate dual SPP focal spots at specific positions, of which phase distribution is shown in Fig. 1(c). The slit patterns without and with the π -phase difference compensation are shown in Figs. 6(a) and 6(c), respectively. The resulting SPP interference patterns from respective slit patterns are presented in Figs. 6(b) and 6(d), respectively. In the case of the circle slit shown in Fig. 6(a), the resulting SPP interference pattern is dual point SPP focus pattern as seen in Fig. 6(b). The π -phase difference between SPPs excited on the Ω_p^+ and Ω_n^+ parts of the slit lead to the destructive interference at the focal points. However, the slit pattern with the π -phase difference compensated is extracted from the form $\Omega_p^+ \cup \Omega_n^-$. The resulting slit pattern and its resulting SPP interference pattern are shown in Figs. 6(c) and 6(d), respectively. As shown in Fig. 6(d), at the focal points, the constructive interference occurs.

Within the framework of the scalar model, the described slit design method is proven to successfully produce two SPP focal spots as well as single SPP focal spot. Using the design method, we can obtain diffractive slit patterns for generating multiple SPP focal spots.

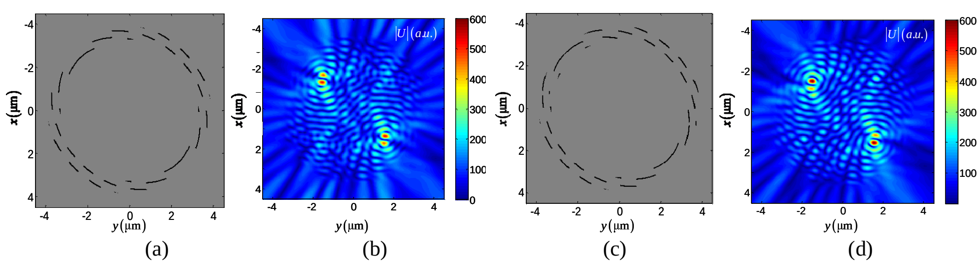

Fig. 6. Two SPP spot generation: (a) slit pattern without the compensation of the π -phase difference, (b) SPP interference pattern, (c) slit pattern with the compensation of the π -phase difference, (d) SPP interference pattern..

3. Numerical results of rigorous coupled wave analysis

In this section, the scalar model based slit pattern design method addressed in Section 2 is tested with the three-dimensional (3-D) RCWA and the scalar model and the 3-D RCWA are comparatively discussed.

All slit patterns used as simulation examples are formed within $9\mu\text{m} \times 9\mu\text{m}$ retangular area on gold (Au) film with a thickness of 300nm . Since we adopt the constant amplitude clipping in the diffractive slit pattern design, for the *x*-directional linear polarization backside incidence, the slit width is kept constant along the *x*-direction without any width variation for specifically modulating the SPP amplitude profile on the slit curves.

In the RCWA, the total number of *x*-directional and *y*-directional Fourier spatial harmonics is set to 61×61 which is the maximum number of harmonics manageable in our

#94111 - $15.00 USD Received 20 Mar 2008; revised 17 May 2008; accepted 30 May 2008; published 3 Jun 2008

personal computer (64bit CPU and 8Gb memory), fortunately, which is the truncation order showing weak convergence, and both the *x*-directional and *y*-directional supercell periods, T_x and T_y, are chosen as a same value of $9\mu m$. Under this setting, the field representation resolution in the $9\mu m \times 9\mu m$ region with 61×61 Fourier spatial harmonics is $150nm \times 150nm$. In the RCWA simulation, the silt width of the tested slit patterns is set to $250nm$ and the real part of the SPP wavelength, λ_{SPP}^{r}, is $616.5nm$. The RCWA resolution of $150nm$ is sufficient to represent the SPP eigenmode on the metal dielectric interface, that is, *z*-directional evanescent 2-D plane waves. Thus the setting is reasonable in representing the slit pattern structures and the generated SPP field distribution inside the concentric band.

Let us consider further the property of the SPP field distribution. We can intuitively know that the SPP field distribution inside the concentric band can be mathematically represented by the superposition of SPP eigenmodes on the metal dielectric interface. It is noted that, in Figs. 7-10, the x-directional and y-directional polarization electric field components inside the concentric band are nearly zero, while the z-directional polarization electric field component is significant. This strongly addresses that the *z*-directional polarization electric field distribution on the surface inside the concentric band can be represented by the scalar expression as

$$E_z(x,y) = \int_C b(x,y) \exp\left(jk_{SPP} \sqrt{(x-x')^2 + (y-y')^2} \right) ds . \tag{9}$$

The complex amplitude $b(x,y)$ is the exact SPP excitation complex coefficient with amplitude and phase values, which can be only obtained by the rigorous vectorial electromagnetic method as the 3-D RCWA. Also, in $b(x,y)$, the multiple reflections between slit patterns, diffraction, and scattering are taken into considered. It is noted that we cannot analyze the complex amplitude $b(x,y)$ using only the scalar analysis. As shown in Eq. (8b), we can only assume the SPP excitation model of Eq. (5) with the aid of physical intuition, where $b(x,y)$ is simply assumed as $\mathbf{p} \cdot \mathbf{n}$. Therefore, in the analysis of diffractive slit patterns, the most distinction point of using the 3D RCWA from using the scalar model should be placed on the fact that the 3D RCWA can provide the exact consideration of $b(x,y)$. The RCWA result shows that the SPP field inside the concentric band is a scalar field with $b(x,y)$ considered fully. It should be understood that the possible difference between the results provided by the scalar model and the rigorous model with respect to the meaning of $b(x,y)$. In fact, the field distributions presented here cannot said to be fully convergent. In general, the convergence of 3D RCWA is practically a hard thing to be attained by conventional personal computers, using which the number of Fourier harmonics retained in computation is seriously limited. However, definitely, as the truncation order increases, the obtained result will be converged at a certain level. However, we can expect that the general focusing feature shown in this paper would not change seriously.

The slit patterns with and without the π-phase difference compensated that generate the single SPP focus at the origin and off-origin are examined with the RCWA. Figures 7(a) and 8(a) show the slit patterns extracted from the prototype slit patterns shown in Figs. 3(a) and 3(c), respectively. In practice, we should find the optimal slit width for efficient SPP excitation. The optimal slit width can be found by repeating parametric simulation with variation in the slit width. After parametric study with the RCWA, we adopted the optimal slit width of $250nm$. The inner rim of the slit pattern is equal to the prototype slit curve, but the outer rim is obtained by translating the inner rim by the slit width, $250nm$. The translation direction is outward from the origin.

#94111 - $15.00 USD Received 20 Mar 2008; revised 17 May 2008; accepted 30 May 2008; published 3 Jun 2008

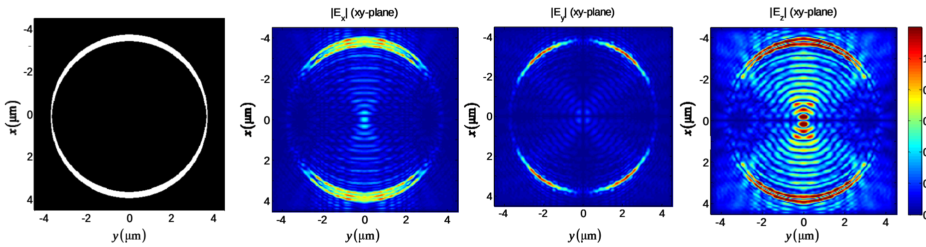

(a) (b) (c) (d)

Fig. 7. RCWA results of single SPP focal spot generation: (a) slit pattern without the π -phase difference compensation, (b) *x*-polarization electric field intensity distribution, (c) *y*-polarization electric field intensity distribution, (d) *z*-polarization electric field intensity distribution

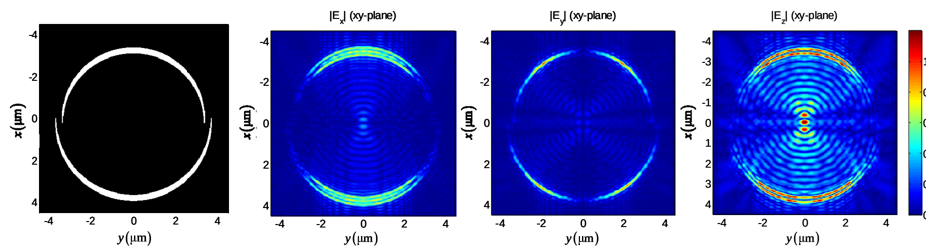

(a) (b) (c) (d)

Fig. 8. RCWA results of single SPP focal spot generation: (a) slit pattern with the π -phase difference compensation, (b) *x*-polarization electric field intensity distribution, (c) *y*-polarization electric field intensity distribution, (d) *z*-polarization electric field intensity distribution

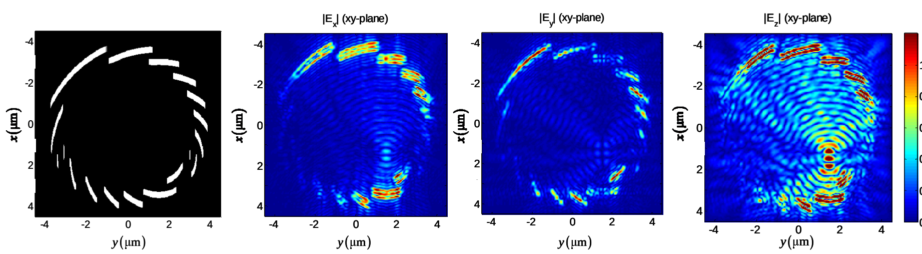

(a) (b) (c) (d)

Fig. 9. RCWA results of off-origin single SPP focal spot generation: (a) slit pattern with the π -phase difference compensation, (b) *x*-polarization electric field intensity distribution, (c) *y*-polarization electric field intensity distribution, (d) *z*-polarization electric field intensity distribution

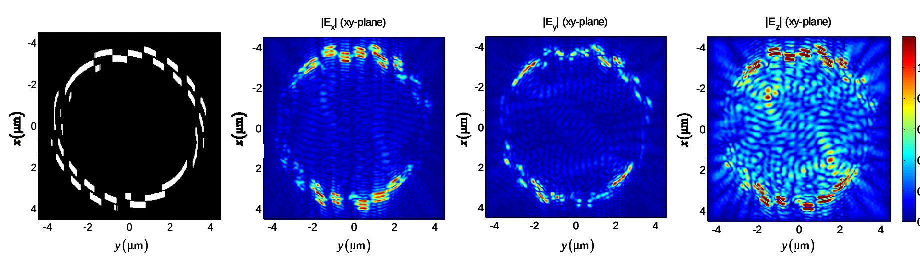

(a) (b) (c) (d)

Fig. 10. RCWA results of two SPP focal spot generation: (a) slit pattern with the π -phase difference compensation, (b) *x*-polarization electric field intensity distribution, (c) *y*-polarization electric field intensity distribution, (d) *z*-polarization electric field intensity distribution

Figures 7(b), 7(c), and 7(d) show the *x*-polarization, *y*-polarization, and *z*-polarization electric field intensity distributions on the front surface of the metal film with the slit without the π-phase difference compensation, respectively, that is analyzed by the 3-D RCWA. In this case, as expected in the scalar model, dual point focus pattern in the *z*-polarization electric field distribution is observed. In Figs. 8(b), 8(c), and 8(d), the *x*-polarization, *y*-polarization, and *z*-polarization electric field intensity distributions obtained from the slit with the π-phase difference compensation are presented, respectively. In this case, because the π-phase difference is compensated in the slit pattern, a single focus pattern appear where the constructive interference occurs at the origin as expected.

Figure 9(a) shows the slit pattern with slit width of 250nm generating the off-origin SPP focal spot, of which prototype pattern is shown in Fig. 5(c). In Figs. 9(b), 9(c), and 9(d), the *x*-polarization, *y*-polarization, and *z*-polarization electric field intensity distributions obtained by the RCWA, are shown, respectively. A single SPP focal spot is formed at the specific position, which is the same position expected by the scalar model. Figure 10 shows the RCWA results of the slit pattern generating two SPP focal spots, of which prototype pattern is shown in Fig. 6(c). In Fig. 10(a), the slit pattern is shown and the *x*-polarization, *y*-polarization, and *z*-polarization electric field intensity distributions are shown in Figs. 10(b), 10(c), and 10(d), respectively. In Fig. 10(d), we can see that two SPP focal spots appear clearly in the *z*-polarization electric field distribution.

Comparing the RCWA results in this section and the scalar model results in the previous section, we can see that the scalar model based diffractive slit pattern design is reasonable. The scalar model expects well the results of the vectorial electromagnetic model although some improvement seems to be needed in the present scalar model.

In this paper, we assume the concentric band where the slit pattern is formed is constrained to $9\mu\text{m}\times 9\mu\text{m}$ square. This restriction is just set for comparing the scalar model and the vectorial electromagnetic model using the RCWA, which is the dimensions for which the 3-D RCWA can produce a reliable analysis result with limited truncation orders of 61×61. As proven in the comparison of the SPP interference patterns obtained by the scalar model and the RCWA, the scalar model based slit pattern design method is a reliable method for real SPP focusing, in particular, multiple SPP focus interference patterns. Although, in this paper, we present two foci generation as an example, with a wider concentric slit band, we can make complex slit patterns producing multiple SPP spots more than two spots.

3. Conclusion

In conclusion, we have proposed a novel design method of diffractive slit patterns for focusing surface plasmon polaritons. The SPP interference patterns expected by the 2-D scalar model and those of the rigorous vectorial electromagnetic analysis are compared and the validity of the scalar model based slit pattern design method has been discussed. The concept presented in this paper would be extended to more general surface plasmon diffractive optical element with complex slit patterns to generate more complex designed SPP field distributions. It is still required to investigate the more accurate scalar model of the SPP diffractive structures with less deviation from the rigorous electromagnetic mode for constructing the efficient optimal design algorithm of SPP diffractive structures.

Acknowledgment

The authors acknowledge the support of the Ministry of Education, Science and Technology of Korea and the Korea Science and Engineering Foundation through the Creative Research Initiative Program (Active Plasmonics Application Systems).

#94111 - $15.00 USD Received 20 Mar 2008; revised 17 May 2008; accepted 30 May 2008; published 3 Jun 2008